A Full Transient ElectroThermal - Elastoplastic Mechanical and Metallurgical 2D FEM of SiC MOSFET for Gate-Region Stress Investigation under Short-Pulse Short-Circuit (Invited)

Mustafa Shqair, Emmanuel Sarraute, Frédéric Richardeau

A Full Transient ElectroThermal - Elastoplastic Mechanical and Metallurgical 2D FEM of SiC MOSFET for Gate-Region Stress Investigation under Short-Pulse Short-Circuit (Invited)

Mustafa Shqair*, Emmanuel Sarraute and Frédéric Richardeau
LAPLACE, University of Toulouse, CNRS, INPT, UPS, Toulouse, France, Email*: mustafa.shqair@laplace.univ-tlse.fr

***Abstract*— As a follow-up to our previous work, the 2D transient Multiphysics electrothermal-mechanical and metallurgical model of a 1.2kV-80mΩ gate-planar SiC MOSFET power chip in a single FEM software, created previously by the authors, has been developed. This model aims to quantify the short-circuit (SC) critical time and energy density of attaining the local dielectric interlayer (ILD) strength and the Al source-metal solidus-liquidus phase transition at elevated temperatures. The novelty of this extended model is considering non-linear electrothermal and elastoplastic material property laws over a wide range of temperatures. Repetitive experimental SC events were carried out to verify the gate-aging occurrence in accordance with the critical values extracted from the proposed model.**

Keywords- SiC MOSFET, Gate-damage, Al's melting, ILD fracture, Multiphysics FEM

I. INTRODUCTION

It is critical to comprehend the SiC MOSFET's limited utilization in extreme operating conditions like SCs before approving crucial applications like aeronautics. The experimentation strategy is the traditional method, but it is undoubtedly expensive to conduct, where it forbids direct physical connections between both the chip-level internal stresses (gate-oxide mechanical strain-stress, electrode melting temperature, thermal runaway, and latch-up through the p-well parasite bipolar transistor) and the external macro stresses applied (typically SC fault time, injected energy, drain-source voltage bias) which cause gate-damages in such power devices (the melting of the source metal and materials' elastoplastic deformations) leading to their failure. As an alternative approach, the authors have developed a complete 2D transient strong coupling Multiphysics FEM fully embedded in Comsol™ software [1].

Previous modeling attempts either lacked clarity in defining the boundary conditions, ignored the Al phase change process, neglected the effect of temperature on the evolution of the material properties over the wide temperature range in SCs, or did not consider the mechanical part, including the elastoplastic behavior of materials [2, 3]. This new study considers for the first time temperature-dependent non-linear i) semiconductor, ii) electrothermal, and iii) elastoplastic materials laws over the wide temperature range in SCs, comprising the Al phase change process. The goal of this paper is to investigate the effect of including the plasticity laws of Al and Ti metallic layers on materials' deformations at the SiC MOSFET half-cell gate region, especially the critical time and energy of interlayer dielectric (ILD) fracture. A comparison was made afterward between our previous model when neglecting the plasticity laws of Al and Ti [1] and the new proposed model when taking such laws into account.

This work presents a continuation to our recently developed Multiphysics FEM technique which is described as follows: in Section II, the static and transient electrothermal models of wide-range SiC MOSFET cell-level are briefly introduced. In Section III, the melting process of Al source-electrode is covered by considering its latent heat of fusion and applying it to the transient electrothermal model built in the previous section. The model was then developed into a transient thermo-mechanical model in Section IV, where the critical pulse time and energy absorption associated with the Al melting and the gate-oxide fracture initiation are quantified. In Section V, the wide-range temperature dependency of all the electrothermal-mechanical properties of materials was applied to the former thermo-mechanical model. The prior thermo-mechanical model was subsequently advanced by incorporating non-linear temperature-dependent plasticity laws for Al and Ti metallic layers in Section VI. Finally, a conclusion is suggested in Section VII.

II. THE BASIC STATIC AND TRANSIENT ELECTROTHERMAL 2D FEMS OF SIC MOSFET HALF-CELL

A. Step one: static electrothermal modeling

In Part A, the basic static electrothermal model is presented. Figure 1 shows the 2D symmetrical device's geometry (its dimensions are listed in Table 1) and doping levels of a generation 2 gate-planar 1.2kV-80mΩ-10.8mm² 4H-SiC N-MOSFET half-cell, with an active area of 6mm², which was fully parametrized physically through Comsol Semiconductor Toolbox™ and referring to Romano *et al.* previous work [4].

Table 1. Geometric dimensions [4]

t_{drift}	14µm	t_{ox}	50nm	t_{poly}	185nm
t_{ild}	416nm	t_{ti}	45nm	t_{al}	4µm
drift	8.7µm	w_{ox}	2µm	w_{poly}	1.77µm
w_{ild}	2.33µm	w_{al}	8.7µm		

M. Shqair, E. Sarraute, F. Richardeau – Lab. Laplace, University of Toulouse, CNRS, INPT, UPS, Toulouse, France, 2024.
IEEE International Reliability Physics Symposium (IRPS) 2024 – Dallas – USA. Invited Paper.
Postprint Accepted Author Manuscript : https://hal.science
doi: 10.1109/IRPS48228.2024.10529493.

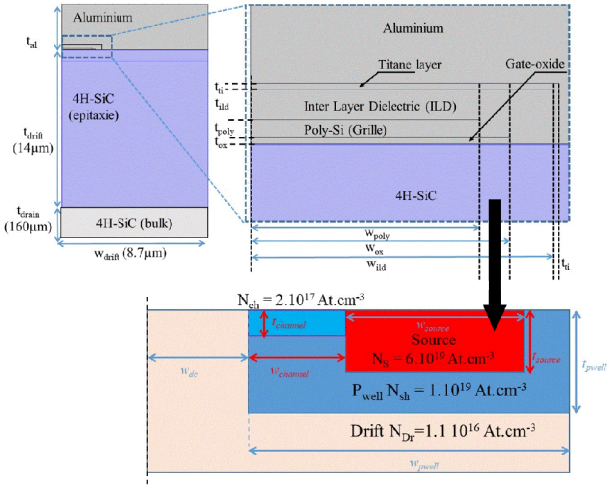

Figure 1. Parametric basis of 1.2kV-80mΩ half-cell gate-planar 4H-SiC MOSFET 2D model

The bulk 4H-SiC material is divided into an intrinsic zone with thickness train and a heavily doped epitaxy zone with thickness drift. This allows for the depletion and spreading of the electric field at the drain-source voltage bias. The top 4H-SiC chip is covered with a 50 nm deposited SiO_2 gate-oxide layer and the poly-Si gate finger. The SiO_2 protective layer called ILD (Internal Layer Dielectric) covers the gate itself, and a thin layer of Ti protects the ILD. ILD provides mechanical protection as well as insulation at the gate-source contact.

Electrical potentials were imposed on the drain, source, and gate electrodes. Electrical isolation was set on the vertical boundaries. Every border had thermal insulation conditions set, and a temperature of 300K was imposed on the drain electrode to represent the cooling state. At this stage, the thin oxide-poly-gate region was simplified using an analogous analytic electrostatic model provided by Comsol™, but only for semiconductor calculus in the SiC. The Gaussian-type doping (or deep junction) profiles were validated after comparing them to those of a basic vertical SiC MOSFET available in the Sentaurus™ library [5]. To properly account for current density gradients, special attention was given to the mesh pitch in the channel region, particularly close to the SiC channel-oxide interface. Indeed, less than 2 nm of thickness is where 80% of the channel current flows!

Electron-hole mobility thermal dependency laws based on the well-known Arora's doping dependency model defined by D. Kim *et al.* [6] for the bulk-channel regions are used. In order to pre-fit the average V_{GSTH} value over 25°C < T_j < 175°C listed in the device datasheet [5], the positive-like fixed oxide-charge density and the negative-like trapping profile interface-charge density were first defined from [4] and then slightly adjusted in combination with channel doping and mobility.

$I_{DS}(V_{GS})$ and $I_{DS}(V_{DS})$ static behaviors at this initial stage are displayed in Figure 2. Rather than precisely fitting the static thermal dependency characteristics, the authors have chosen to concentrate more on the transient channel-current global fitting, which will serve as the foundation for the metallurgical and thermomechanical modeling using the channel's mobility parameter, as will be described in Part B.

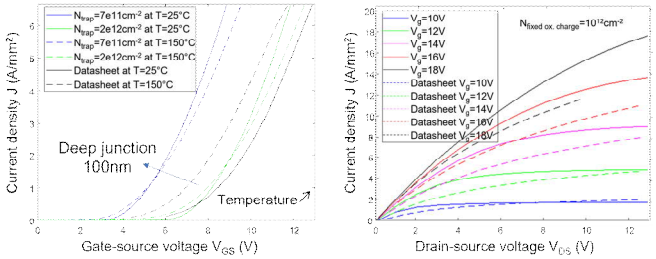

Figure 2. Static results of 1.2kV-80mΩ half-cell gate-planar 4H-SiC MOSFET 2D model

The simulation results appear physically reasonable, but they have not pursued a static mode with greater accuracy because Part B of the study will require a re-adjustment of the model using the channel's mobility parameter at a high transient temperature, which is critical for achieving the gate-region metallurgical and thermal-stress investigation.

B. Step two: transient electrothermal modeling

Temperature dependency laws for 4H-SiC intrinsic carrier density $n_i(T)$ and the thermal properties of all materials, such as the heat capacity (C_p) and thermal conductivity (λ), were defined in compliance with [6]. In fact, extending them across such a high-temperature range as in SC operations is not simple. This also holds for the charge-trapping/de-trapping and mobility laws mentioned in Part A. In order to tackle this issue, the authors have accounted for all of these complicated variations by introducing in (2) an extra thermal-dependent mobility adjustment law, $\mu_{adj}(T_j)$, derived from the well-known Arora's law (1) [4] as presented in Figure 3.

$$\frac{1}{\mu_{channel}} = \frac{1}{\mu_{Arora}\,(T, N_D, N_A)} + \frac{1}{\mu_{adj}} \tag{1}$$

$$\mu_{adj} = \mu_{0,pl}\left(\frac{T}{T_{ref}}\right)^{\alpha_{PLM}} \tag{2}$$

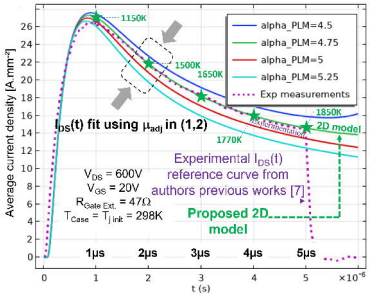

Figure 3. Short-circuit transient $I_{DS}(t)$ conditions and law normalized on the active area of 6mm²

According to Figure 3, such a coefficient is effectively employed to fully fit the $I_{DS}(t)$ channel saturation wave on the experimental response from earlier authors' work (Figure 4-a in [7]). Keep in mind that this model lacks Shockley-Read-Hall generation-type leakage current at high temperatures and V_{DS} bias. Accordingly, this paper does not model the drain-source leakage current. Nevertheless, this does not detract from our analysis, which focuses on the thermal stress surrounding the gate region, where damages take place early there during SCs, as we will conclude later from this study.

M. Shqair, E. Sarraute, F. Richardeau – Lab. Laplace, University of Toulouse, CNRS, INPT, UPS, Toulouse, France, 2024.
IEEE International Reliability Physics Symposium (IRPS) 2024 – Dallas – USA. Invited Paper.
Postprint Accepted Author Manuscript : https://hal.science
doi: 10.1109/IRPS48228.2024.10529493.

III. TRANSIENT THERMAL BEHAVIOR OF THE AL GATE-SOURCE ELECTRODE WHEN INCLUDING ITS PHASE TRANSITION

A source-electrode melting model is necessary because of the lower melting temperature of Al (933K) in comparison to the SiC channel temperatures involved in SCs (>1200K). Furthermore, Al will operate as a high-energy heat sink because of its relatively high metal thickness, delaying the temperature rise time around the gate region and impacting the strain-stress behavior over there.

The Al solidus-liquidus phase change modeling is applied to the earlier 2D transient electrothermal model detailed in Section II.B. The suggested melting model is based on the application of an analytic Gaussian transition law, which was recently implemented for the first time in 2D by authors in [8,9], to introduce the metal's specific latent heat (L_f = 397 kg/K) over a solidus-liquidus temperature range (933K ± $\Delta\theta_f$) as shown in Figure 4, where $\Delta\theta_f$ = 15 K. Using the same strategy, solidus-liquidus non-linear laws of Al's thermal conductivity and density were introduced, based on the parameters in Table 2, which also contains the material properties for Ti, SiO_2, poly-Si, and 4H-SiC.

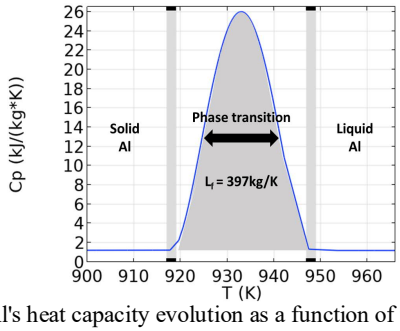

Figure 4. Al's heat capacity evolution as a function of temperature

Table 2. A summary of the material properties used in Section III [9]

Property	Al (solid)	Al (liquid)	Ti	SiO_2	Poly-Si	4H-SiC
ρ (Kg/m^3)	2700	2370	4506	2200	2320	3210
λ (W/m.K)	237	100	21.9	1.4	34	340
Cp (kJ/kg.K)	0.9	1.175	0.522	0.73	0.678	0.75

For a SC of 5µs, the evolution of the 2D transient thermal maps is displayed in Figure 5-a. The hot spot moves quickly from its initial location in the JFET inter-cell region to the source region at the channel-source side then diffuses to the gate region. The very small dimensions and strong internal gradient make it difficult to visualize the thermal analysis within the channel graphically.

Upon reaching the solidus-liquidus transition band at t = 2.55µs at the SiC-Al interface, Figure 5-b displays a remarkable dynamic "wave-like melting-front spreading" throughout the entire source-electrode thickness. At t = 5.15µs, the melting front eventually reaches the top of the source-electrode after straightening towards the gate's axis, which becomes a hot region. After 7µs, some regions start re-solidification caused by the decrease in the temperature. A practical top view is shown in an inset photo, which demonstrates the metal swelling caused by a full source melting under the same operating conditions.

The critical energy density at t = 2.55µs, which is equal to 270mJ/6mm² = 4.5J/cm², can finally be extracted from Figure 5-c, resulting in a junction temperature T_j = 1420K, thanks to the correlation between this transient thermal analysis and the semiconductor electrical model from Section II.B, and the authors' experimentation for a SC of 2.5µs [7]. The metal will undergo local melting cycles with each SC beyond this critical time and energy density absorption. This will severely degrade the source-electrode and possibly lead to Al's diffusion through the ILD-SiO_2 formed cracks or even its vaporization, over-compressing the oxide-poly-gate, as will be examined in the upcoming section.

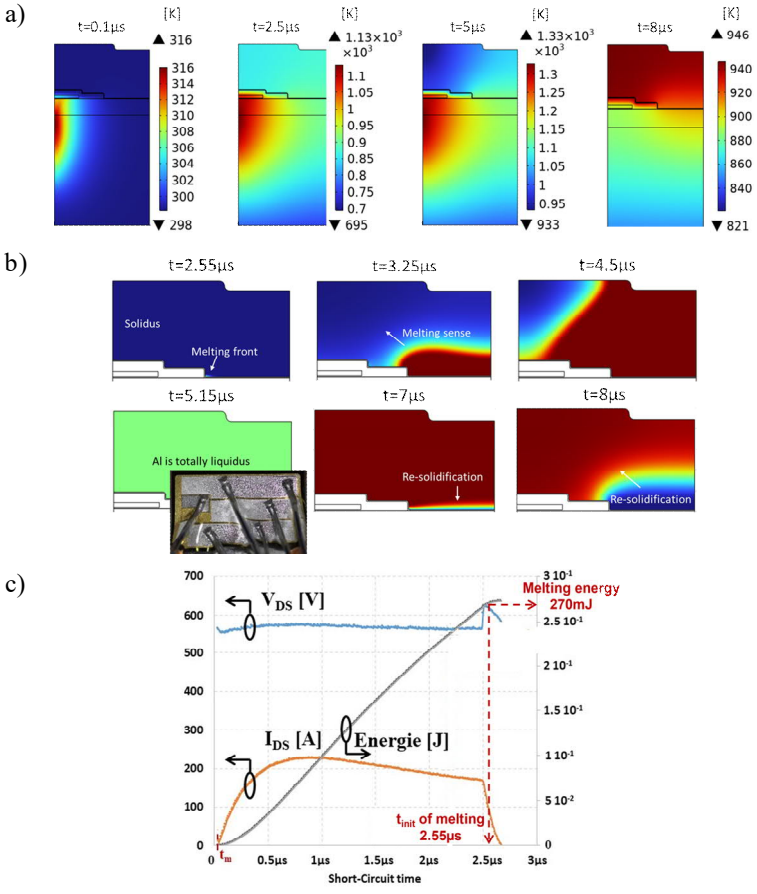

Figure 5. a) 2D transient thermal simulation {V_{DS} = 600V, V_{GS} = 20V, T_{CASE} = 25°C} including a solid-liquid melting model of Al, b) Dynamic melting front across the Al layer, c) Melting time and energy absorption based on the electrothermal modeling and authors experimentation [7]

IV. TRANSIENT THERMOMECHANICAL RESPONSE (ELASTIC) AND GATE'S STRESS ANALYSIS UNDER SC

This section seeks to take advantage of the prior model to conduct a preliminary analysis of the gate region's thermomechanical properties and behavior in SC operation in correlation with the authors' previous experimental findings obtained on the same DUT. In particular, the critical time and energy of the ILD-Ti layer's mechanical strength will be

M. Shqair, E. Sarraute, F. Richardeau – Lab. Laplace, University of Toulouse, CNRS, INPT, UPS, Toulouse, France, 2024.
IEEE International Reliability Physics Symposium (IRPS) 2024 – Dallas – USA. Invited Paper.
Postprint Accepted Author Manuscript : https://hal.science
doi: 10.1109/IRPS48228.2024.10529493.

extracted after being able to extract the melting time and energy in the preceding section. The significance of these data appears to lie in their ability to draw attention to aging boundaries and set a maximum protection time for the gate-driver to avoid SiC MOSFET degradations in repetitive SCs over a broad cycle number. As a first basic approach, all SiC MOSFET thermal and mechanical parameters have constant values, as described in Table 2 and Table 3.

Table 3. Mechanical properties of materials at 300 K [2,17]

Material	Fracture strength (GPa)	CTE (10^{-6}/K)	Young modulus (GPa)	Poisson ratio
Al	0.15	23	70	0.33
Ti	0.95±0.15	8.6	115.7	0.321
SiO_2	1	0.5	70	0.17
Poly-Si	1.2-3.0	2.6	160	0.22
4H-SiC	21	4.3	500	0.157

It is preferable to use distinct mesh sizes because the intensity and distribution of mechanical and electrical gradients greatly differ. To accurately describe the channel's current density, the JFET and channel regions impose sub-nanometric electric meshes, while nanometric mechanical meshes are required only in Ti and SiO_2 layers to account for the stress gradient. Very promising results were obtained using a dedicated re-meshing of the gate region, done with a re-interpolation between the transient thermal map in the electrical mesh used in Section III and the new mechanical mesh used in this section under weak coupling mode.

As observed in Figure 6-a, it is consistent to note that the maximum mechanical stress regions are localized close to the hottest SiC-Ti-Al source-electrode zone and around the geometric singularities of the ILD-Ti zone. In particular, the ILD-Ti region exhibits strong mechanical stress due to the strong CTE differential at the Al-Ti interface imposed by the thick Al bulk source electrode and generated by the strong Ti's Young modulus value. Actually, it is difficult to assume a specific value for the SiO_2's fracture stress, where it highly differs in the literature, depending on its thickness, porosity, crystal structure, etc. (0.6-2.3GPa) [2,3,10]. A value around 0.8GPa was found in the literature for SiO_2 layers used in microelectronic applications with a thickness close to that used in our model; consequently, this value will be considered in this study [10,11]. At this Al-Ti interface, the SiO_2 strength of 0.8GPa is exceeded, which may cause a crack to initiate and spread from the Al-Ti barrier to the poly-Si gate finger. Using FIB and SEM, in collaboration with THALES SIX France and CNES laboratories, the authors observed ILD-SiO_2 corner cracks, which are visually consistent with the simulated stress values at the Al-Ti interface. The stress values and distribution, accompanied by additional interpretations and correlations with experimental tests, are to be validated in the next section, where the model will be more accurate after considering the temperature effect on the evolution of the material properties. Figure 6-b shows the selected cut-points at the positions of interest for doing the temperature-stress evolution interpretation inside materials for this section and the upcoming ones. Using Figure 6-c, it is deduced that Al's melting starts at 2.55µs, and the SiO_2 strength is exceeded at 1.6µs when looking at point A.

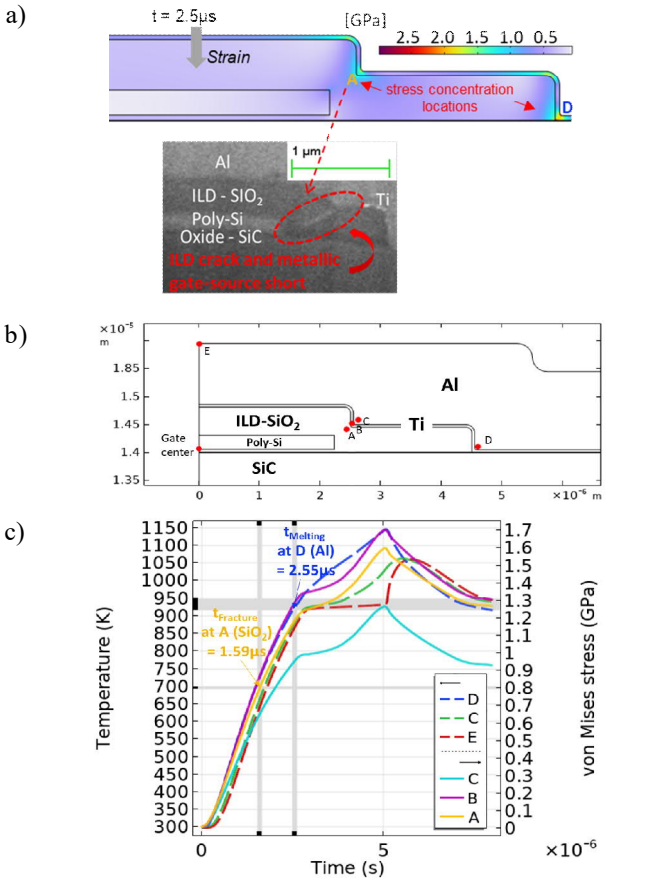

Figure 6. a) Surface stress distribution, b) Cut-points selected for stress, strain, and temperature evolution analysis in this paper, c) Temperature-stress evolution at cut-points in the transient thermomechanical (elastic) simulation in SC operation {V_{DS} = 600V, V_{GS} = 20V, T_{CASE} = 25°C} with material properties at 300K

V. Considering Temperature-Dependent Thermal and Mechanical Properties for All Materials in the Transient Thermomechanical Model (Elastic)

Temperature changes can significantly impact the properties of SiC substrate and gate-region materials. Materials would behave differently in SiC MOSFETs due to the wide temperature range (300-1500K) in SCs. The most significant property laws that could be impacted are the CTE and Young modulus of the thick Al source electrode. Thus, it would be crucial to look into the deformation behavior at the interfaces between Al, Ti, ILD, and SiO_2, particularly in the area where cracks form and the Al phase transition takes place. The large temperature range may, therefore, impact the critical times of energy and mechanical strength.

According to [12, 13], Al CTE changes from 23ppm/K at 300K in the solid state to 110ppm/K in the liquid state. Its Young Modulus E(T) also changes from 70GPa at 300K in the solid state to null in the liquid state! The authors proposed modeling such a sudden change by physically integrating the Gaussian law used for Al's $C_p(T)$ over the solidus-liquidus temperature range in Section III, as presented in Figure 4. This was done by utilizing the smoothed error-type special function erf(x) shown in equations (3) and (4).

M. Shqair, E. Sarraute, F. Richardeau – Lab. Laplace, University of Toulouse, CNRS, INPT, UPS, Toulouse, France, 2024.
IEEE International Reliability Physics Symposium (IRPS) 2024 – Dallas – USA. Invited Paper.
Postprint Accepted Author Manuscript : https://hal.science
doi: 10.1109/IRPS48228.2024.10529493.

$$\alpha(T) = \frac{1}{2}\left(1 + \mathrm{erf}\left(\frac{T - T_f}{\sigma\sqrt{2}}\right)\right) \quad (3)$$

$$\mathrm{erf}(x) = \frac{2}{\sqrt{\pi}}\int_0^x e^{-t^2}\,dt \quad (4)$$

By which T is the temperature in K, T_f is the melting point of Al, which is 933K, σ is the standard deviation that is fixed at σ = 5K, and t is the time in s.

By using this smoothed transition of material properties, the calculus convergence is softened. As a result, the material properties of Al were defined as a function of α(T) as illustrated in equation (5) and Figure 7, where "Prop" stands for either the poisson ratio (ν), the Young modulus (E), the thermal expansion coefficient (CTE), heat capacity (C_p), thermal conductivity (λ), or density (ρ). Note that since both E and ν do not exist in liquids, very low values were assumed for these parameters for Al's liquid state to smoothen the calculus convergence.

$$\mathrm{Prop}(T) = \mathrm{Prop}_{\mathrm{solid}}(T) * \left(1 - \alpha(T)\right) + \mathrm{Prop}_{\mathrm{liquid}}(T) * \alpha(T) \quad (5)$$

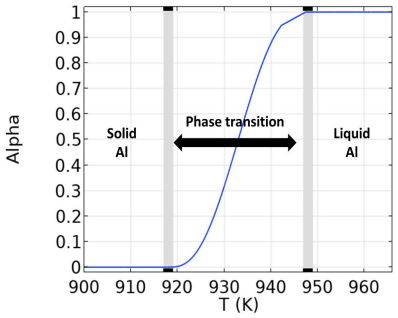

Figure 7. Al's transition factor α(T)

a)

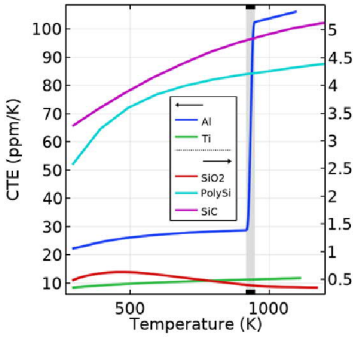

b)

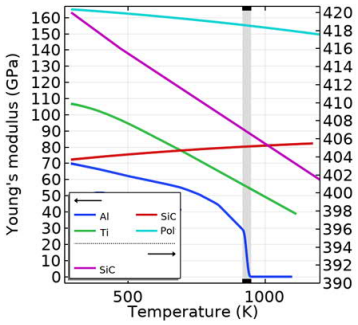

c)

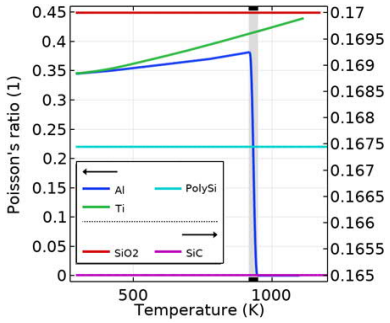

Figure 8. The evolution of a) CTE, b) Young modulus and c) Poisson ratio as a function of temperature for Al, SiO_2, Ti, SiC, and poly-Si [1]

a)

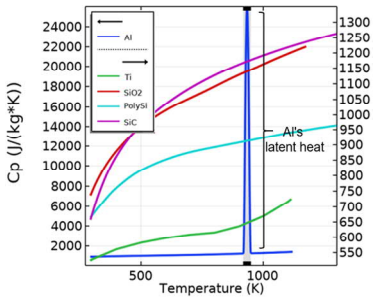

b)

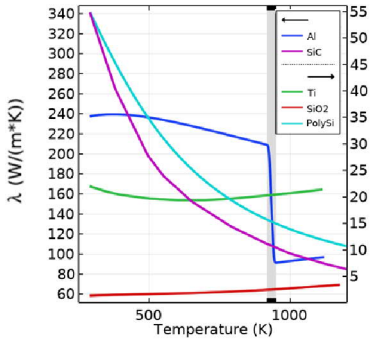

c)

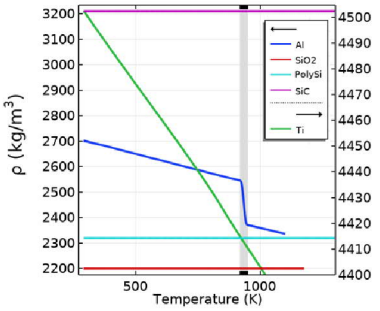

Figure 9. The evolution of a) Heat capacity, b) Thermal conductivity and c) Density as a function of temperature for Al, SiO_2, Ti, SiC, and poly-Si [9]

The CTE, E, and ν mechanical laws for the materials Al, SiO_2, Ti, poly-Si, and SiC are displayed as a function of temperature in Figure 8 [1]. Additionally, the evolution of the C_p, λ, and ρ thermal properties as a function of the temperature of each of these materials is also taken into account, as presented in FIGURE 9, after improving the authors' electrothermal model in [9]. In these figures, the gray area denotes the Al melting zone.

M. Shqair, E. Sarraute, F. Richardeau – Lab. Laplace, University of Toulouse, CNRS, INPT, UPS, Toulouse, France, 2024.
IEEE International Reliability Physics Symposium (IRPS) 2024 – Dallas – USA. Invited Paper.
Postprint Accepted Author Manuscript : https://hal.science
doi: 10.1109/IRPS48228.2024.10529493.

A complete simulation of the upper assembly, including the thick epoxy case and the thin Si_3N_4 barrier layer, is still pending. In this simulation, symmetry boundary conditions were fixed on the vertical borders, and zero displacements were imposed on the upper and lower borders. The updated map and chronogram of temperature and stress at the positions of interest are displayed in Figure 10.

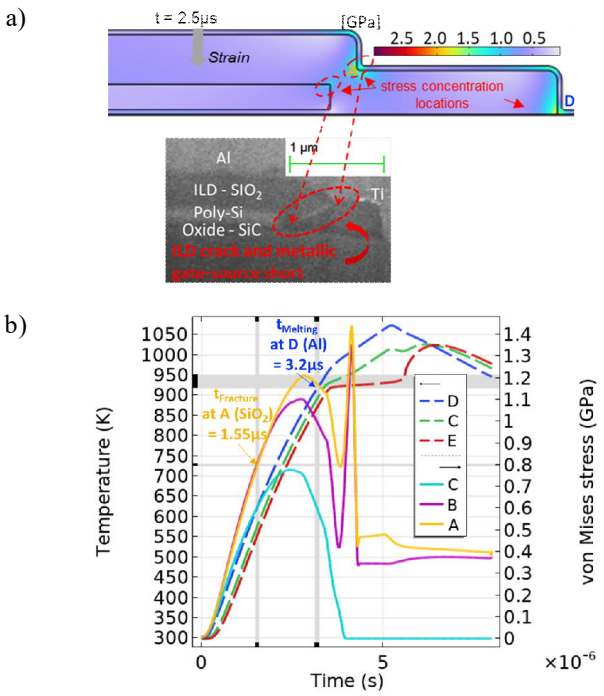

Figure 10. a) Surface stress distribution and b) Temperature-stress evolution at cut-points in the transient thermomechanical (elastic) simulation with temperature-dependent material properties in SC operation {V_{DS} = 600V, V_{GS} = 20V, T_{CASE} = 25°C}

Similar to Figure 6, stress concentrates at the SiC-Ti-Al and ILD-Ti zones, as observed in Figure 10-a. It is visually noticeable that the edges of the oblique crack have a stress exceeding the SiO_2 strength, which is much more consistent with the experimentally observed ILD-SiO_2 corner cracks.

In Figure 10-b, a focus is dedicated to the chronograms of the temporal transient mechanical stresses at the positions of interest. This graph is highly interesting because it lets us understand what is happening. At the beginning of a SC, the overall temperature rises in the structure, causing an increase in the CTE of materials. That raises the stress in materials. Prior to the onset of Al's melting, the reduction in Al's Young modulus attenuates the dynamic increase in the Ti barrier and ILD-SiO_2 stresses. When Al's melting starts, the accelerated decrease in Al's Young modulus leads to a drop in all resulting stresses on the Ti barrier and ILD-SiO_2. However, this Al's Young modulus drop is simultaneous with the sharp rise in its CTE and the significant CTE differential between Ti and ILD-SiO_2. That resulted in the stress peaks just after. Due to the temperature drop and Al's CTE saturation, progressive stress stabilization occurs at the final state until Al melts completely.

A delay in Al's melting resulted in when comparing Figure 6 (2.55µs) with Figure 10-b (3.2µs) as well as a decrease in the global Al temperature values is observed due to the decrease of the thermal diffusivity in materials within temperature, reducing the heat flow transmitted to the Al. Moreover, stress chronograms have undergone substantial modification. This is because, as Figure 8 demonstrates, Al's Young modulus decreases from 750K onward and collapses at 933K, in addition to the strong increase in its CTE (x5) from 300K to 933K.

VI. Transient Thermomechanical Response (Elastoplastic) and Gate's Stress Analysis under SC

This model has the same conditions as the model in the previous section but includes plasticity laws that respect the temperature-wide range during SCs for metals. In this section, temperature-dependent bilinear kinematic elastoplastic laws are applied to Al and Ti as schematized in Figure 11-a (Young modulus for the elastic zone (Figure 8-b), yield strength for the zone separating the elastoplastic region (Figure 11-b), and an isotropic tangential slope for the plasticity domain (Figure 11-c)) [14-16].

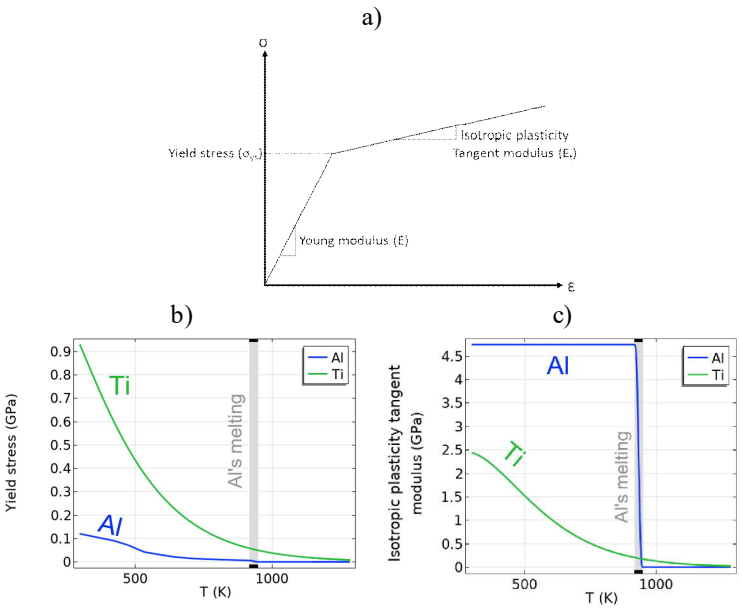

Figure 11. Elastoplastic properties of Al and Ti [14-16]

The importance of considering such laws is that they will strongly affect the stress-strain and deformation behaviors in the materials at the gate region. It will also be important for the continuation of this work, where the next step is to model the ILD fracture. It is critical to consider Ti's plasticity due to the high impact of temperature on its yield strength. We can see a very high decrease in its yield stress and plasticity tangent modulus as the temperature increases, and this is very clear before reaching the temperature of Al's melting. Regarding Al, much attention should be paid to its defined plasticity law because it will only be valid for its solid state. Its plastic properties will collapse when Al melts at 933K.

Concerning the model's preliminary results, much higher strains are present when including plasticity after comparing

M. Shqair, E. Sarraute, F. Richardeau – Lab. Laplace, University of Toulouse, CNRS, INPT, UPS, Toulouse, France, 2024.
IEEE International Reliability Physics Symposium (IRPS) 2024 – Dallas – USA. Invited Paper.
Postprint Accepted Author Manuscript : https://hal.science
doi: 10.1109/IRPS48228.2024.10529493.

the resulting strains in the model of the previous section (pure elastic) in FIGURE 12-a to those in the new model (elastoplastic) in FIGURE 12-b, especially just before and after Al's melting. Note that in both cases, Al's strain becomes very high compared to that of Ti after the initiation of its melting.

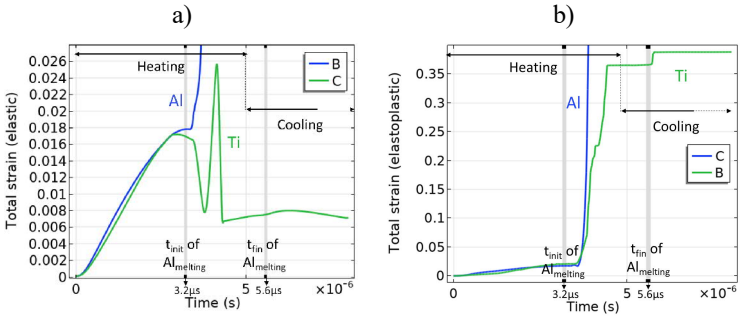

Figure 12. Strain evolution with time at cut-points b (Ti) and c (Al) in the models of sections a) V (Elastic) and b) VI (Elastoplastic)

The new evolutions of stress and temperature are shown in FIGURE 13-a. It is observed that the decrease of Ti and Al stresses, just before Al's melting initiation at 3.2µs, occurs earlier compared to that in our previous model when looking at Figure 10. The maximal stresses reached in this new model are lower, and the SiO_2 fracture stress value listed in the literature (0.8GPa [10,11]) is reached in the new model at 3.95µs after Al's melting. Undoubtedly, including the plasticity criterion plays a critical but proper role in reducing stresses; however, with and without including it, this stress peak is always present and is most probably due to the strong increase in Al's CTE and the resulting critical CTE differential at the Al-Ti-SiO_2 region. That caused the elevated rise in Al's and Ti's strains just after the melting initiation of Al, as observed in FIGURE 12-b. At the time of the stress peak, FIGURE 13-b illustrates that the stress-concentration positions are the locations of cracks seen experimentally at the ILD-Ti region. Therefore, FIGURE 13 (a and b) is highly important because it can clearly highlight the suggested melting and cracking scenarios chronologically, where molten/softened Al may pass through the fractured ILD based on physical evidence and the simulation results.

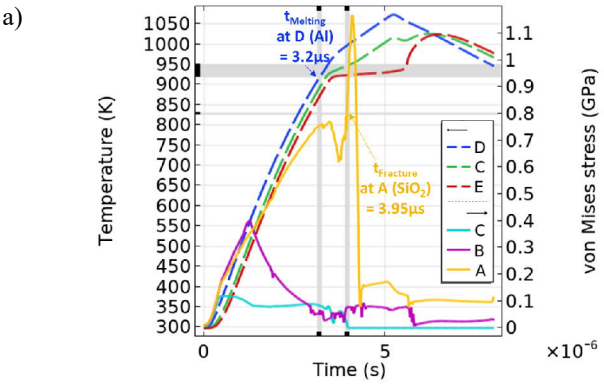

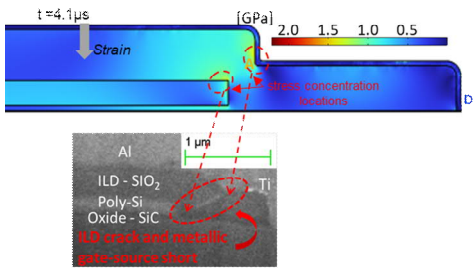

Figure 13. a) Temperature-stress evolution at cut-points, and b) Surface stress distribution in the transient thermomechanical (elastoplastic) simulation with temperature-dependent material properties in SC operation {V_{DS} = 600V, V_{GS} = 20V, T_{CASE} = 25°C}

When looking at FIGURE 14-a, it can be deduced that the direction of displacement in poly-Si is inversed just after the melting initiation of Al. Before Al's melting, the poly-Si displacement was directed downwards as if Al was exerting a pushing action. When Al starts melting, fewer constraints have resulted at the topside due to the liquidation of Al, which causes the upward poly-Si displacement. This upward displacement is also forced by the topside pushing action of the upper part of the SiC bulk at which the temperature concentrates and is enhanced by the high variation in terms of Young modulus and CTE at the SiC-poly-Si region. As observed in FIGURE 14-b, it is clear that the sharp increase in the stress at point A (SiO_2) starting from 3.8µs toward its maximum value at 4.12µs (passing through its fracture stress at 3.95µs) is synchronous with the intense increase in the poly-Si displacement in its upward direction. Accordingly, the deformations of poly-Si have a high impact on the fracture of SiO_2.

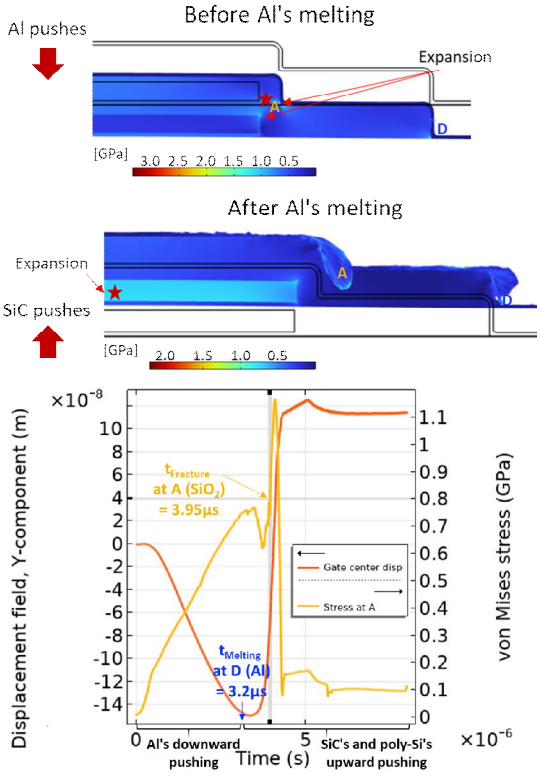

M. Shqair, E. Sarraute, F. Richardeau – Lab. Laplace, University of Toulouse, CNRS, INPT, UPS, Toulouse, France, 2024.
IEEE International Reliability Physics Symposium (IRPS) 2024 – Dallas – USA. Invited Paper.
Postprint Accepted Author Manuscript : https://hal.science
doi: 10.1109/IRPS48228.2024.10529493.

Figure 14. The evolution of a) Surface deformations and b) Displacement-stress evolution at gate center and ILD-SiO_2 cut-points, respectively, in the transient thermomechanical (elastoplastic) simulation with temperature-dependent material properties in SC operation {V_{DS} = 600V, V_{GS} = 20V, T_{CASE} = 25°C}

Lastly, in Figure 15, the authors performed experimental repetitive SCs on a dedicated test bench [7] to confirm the existence of a mechanical rupture threshold of the ILD-SiO_2. A short-pulse SC 2.5µs (left side) around the critical time and a long-pulse SC 5µs (right side) greater far from the critical time were considered. The device can withstand a set of 1000 SC in a short pulse without exhibiting any apparent gate-source leakage current or drain-source channel transient conduction degradation. On the other hand, the device clearly exhibits a permanent gate-source leakage current from the two-hundredth cycle and drain-source channel transient conduction degradation during long pulses.

In fact, when ignoring the effect of temperature on the evolution of the material properties and when neglecting the plasticity effect, the stress peak was achieved prior to 2.5µs. Accordingly, it could be interesting to note that exclusively in this last complete model, both the stress peak and the start of Al's melting are achieved after 2.5µs, as shown in FIGURE 13-a. This justifies why, at 2.5µs, no degradations were observed experimentally in Figure 15, whereas at 5µs, gate-damage associated with the Schottky emission arose. These findings may demonstrate that, in order to prevent degradations, the gate-driver's SC protection delay must function in a time lower or equivalent to the critical times of Al melting (3.2µs) and SiO_2 cracking (3.95µs). Undoubtedly, this new model resulted in a positive step for the structure's mechanical robustness since the close control has more time to secure the component when an SC is detected and thus avoids mechanical degradation at the gate region.

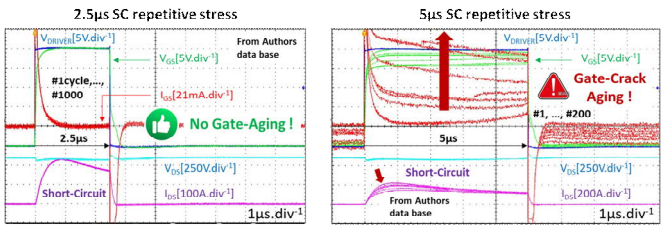

Figure 15. Repetitive electrical SC gate-damage from authors' test bench

VII. CONCLUSIONS

The previous 2D transient Multiphysics metallurgical and electrothermal-mechanical FEM proposed by the authors of SiC MOSFET 1.2kV-80mΩ has been extended and investigated by including the Al and Ti plasticity criterion [1,9]. This model includes temperature-dependent laws of all physical parameters over a very wide temperature range (300-1500K) and considers the melting modeling of Al. Compared to earlier modeling methods described in the literature, this model delivers substantial improvements. Compared to our previous attempt, it was observed that plasticity undoubtedly limited the stress field and affected reaching the ILD fracture stress [1]. Adjusting the temperature-dependent laws for the thermal properties of materials retarded the Al's melting initiation [9]. This complete and global modeling approach looks fundamental for designers, enabling them to extract numerically the critical thermal and mechanical gate-damage times of SiC MOSFETs to optimize gate-driver protection and possibly redesign the device to be more robust. The current model undoubtedly needs to be completed by considering the topside protective layers to better consider the mechanical constraints and is to be followed by crack gate-damage modeling, which could be useful for predicting the maximum number of cycles to failure.

REFERENCES

[1] M. Shqair *et al.,* "Thermo-mechanical and metallurgical preliminary analysis of SiC MOSFET gate-damage mode under short-circuit based on a complete transient multiphysics 2D FEM." Microelectronics Reliability 150 (2023): 115081.

[2] J. Liu *et al.,* "Gate failure physics of SiC MOSFETs under short-circuit stress." IEEE Electron Device Letters 41, no. 1 (2019): 103-106.

[3] T. Shoji *et al.* "Dependence of short-circuit withstand capability of SiC MOSFETs on short-circuit failure time." IEEE Transactions on Power Electronics 36, no. 10 (2021): 11739-11747.

[4] G. Romano *et al.* "A comprehensive study of short-circuit ruggedness of silicon carbide power MOSFETs." IEEE Journal of Emerging and Selected Topics in Power Electronics 4, no. 3 (2016): 978-987.

[5] T. Cazimajou *et al.* "On the Electro-Thermal 2D FEM Parametric Analysis of SiC Vertical MOSFET Including Gate-Oxide Charge-Trapping Thermal Dependency: Application for Fast Transient Extreme Short-Circuit Operation." In 30th International Conference on Mixed Design of Integrated Circuits and System (MIXDES), pp. 212-217. IEEE, 2023.

[6] D. Kim *et al.* "Non-isothermal simulations to optimize SiC MOSFETs for enhanced short-circuit ruggedness." In IEEE International Reliability Physics Symposium (IRPS), pp. 1-6. IEEE, 2020.

[7] W. Jouha *et al.* "Repetitive short circuit capability of SiC MOSFET at specific low gate-source voltage bias for more robust extreme operation." Microelectronics Reliability 126 (2021): 114253.

[8] E. Sarraute *et al.* "Transient Thermal 2D FEM Analysis of SiC Mosfet in Short-Circuit Operation Including Solidus-Liquidus Phase Transition of the Aluminum Source Electrode." In 24th International Conference on Thermal, Mechanical and Multi-Physics Simulation and Experiments in Microelectronics and Microsystems (EuroSimE), pp. 1-8. IEEE, 2023.

[9] M. Shqair *et al.*, "Transient Thermal 2D FEM Analysis of SiC Mosfet in Short-Circuit Operation Including High-temperature Material Laws and Phase Transition of Aluminum Source Electrode." submitted to Microelectronics Reliability (2024).

[10] V. Hatty *et al.* "Fracture toughness, fracture strength, and stress corrosion cracking of silicon dioxide thin films." Journal of microelectromechanical systems 17, no. 4 (2008): 943-947.

[11] T. Tsuchiya *et al.* "Tensile testing of insulating thin films; humidity effect on tensile strength of SiO2 films." Sensors and Actuators A: Physical 82, no. 1-3 (2000): 286-290.

[12] K. Wang *et al.* "The perfect crystal, thermal vacancies and the thermal expansion coefficient of aluminium." Philosophical Magazine A 80, no. 7 (2000): 1629-1643.

[13] J. Puigcorbé *et al.* "Thermal fatigue modeling of micromachined gas sensors." Sensors and Actuators B: Chemical 95, no. 1-3 (2003): 275-281.

[14] W. Kanert *et al.* "Modelling of metal degradation in power devices under active cycling conditions." In 12th Intl. Conf. on Thermal, Mechanical & Multi-Physics Simulation and Experiments in Microelectronics and Microsystems, pp. 1-6. IEEE, 2011.

[15] H. Shahmir *et al.* "Mechanical properties and microstructural evolution of nanocrystalline titanium at elevated temperatures." Materials Science and Engineering: A 669 (2016): 358-366.

[16] Piping Process. "ASME B31. 3." The American Society of Mechanical Engineers: New York, NY, USA (2010).

[17] W. N. Sharpe, "Mechanical Properties of MEMS Materials," in The MEMS Handbook, vol. 3. Boca Raton, FL, USA: CRC Press, 2002, pp. 49–54.

M. Shqair, E. Sarraute, F. Richardeau – Lab. Laplace, University of Toulouse, CNRS, INPT, UPS, Toulouse, France, 2024.
IEEE International Reliability Physics Symposium (IRPS) 2024 – Dallas – USA. Invited Paper.
Postprint Accepted Author Manuscript : https://hal.science
doi: 10.1109/IRPS48228.2024.10529493.